

A Unique Cellular Organization of Human Distal Airways and Its Disarray in Chronic Obstructive Pulmonary Disease

Samir Rustam^{1*}, Yang Hu^{2*}, Seyed Babak Mahjour¹, Andre F. Rendeiro², Hiranmayi Ravichandran², Andreacarola Urso³, Frank D'Ovidio³, Fernando J. Martinez¹, Nasser K. Altorki⁴, Bradley Richmond^{5,6}, Vasily Polosukhin⁵, Jonathan A. Kropski^{5,6}, Timothy S. Blackwell^{5,6}, Scott H. Randell⁷, Olivier Elemento², and Renat Shaykhiev¹

¹Department of Medicine and ²Caryl and Israel Englander Institute for Precision Medicine, Department of Physiology and Biophysics, Weill Cornell Medical College, New York, New York; ³Department of Surgery, Columbia University Irving Medical Center, New York, New York; ⁴Department of Cardiothoracic Surgery, Weill Cornell Medicine, New York, New York; ⁵Department of Veterans Affairs Medical Center, Nashville, Tennessee; ⁶Department of Medicine, Vanderbilt University, Nashville, Tennessee; and ⁷Marsico Lung Institute, The University of North Carolina at Chapel Hill, Chapel Hill, North Carolina

ORCID IDs: 0000-0001-6200-5235 (B.R.); 0000-0001-8945-548X (R.S.).

Abstract

Rationale: Remodeling and loss of distal conducting airways, including preterminal and terminal bronchioles (pre-TBs/TBs), underlie progressive airflow limitation in chronic obstructive pulmonary disease (COPD). The cellular basis of these structural changes remains unknown.

Objectives: To identify biological changes in pre-TBs/TBs in COPD at single-cell resolution and determine their cellular origin.

Methods: We established a novel method of distal airway dissection and performed single-cell transcriptomic profiling of 111,412 cells isolated from different airway regions of 12 healthy lung donors and pre-TBs of 5 patients with COPD. Imaging CyTOF and immunofluorescence analysis of pre-TBs/TBs from 24 healthy lung donors and 11 subjects with COPD were performed to characterize cellular phenotypes at a tissue level. Region-specific differentiation of basal cells isolated from proximal and distal airways was studied using an air-liquid interface model.

Measurements and Main Results: The atlas of cellular heterogeneity along the proximal-distal axis of the human lung was assembled and identified region-specific cellular states, including *SCGB3A2*⁺ *SFTPB*⁺ terminal airway-enriched secretory cells (TASCs) unique to distal airways. TASCs were lost in COPD pre-TBs/TBs, paralleled by loss of region-specific endothelial capillary cells, increased frequency of CD8⁺ T cells normally enriched in proximal airways, and augmented IFN- γ signaling. Basal cells residing in pre-TBs/TBs were identified as a cellular origin of TASCs. Regeneration of TASCs by these progenitors was suppressed by IFN- γ .

Conclusions: Altered maintenance of the unique cellular organization of pre-TBs/TBs, including loss of the region-specific epithelial differentiation in these bronchioles, represents the cellular manifestation and likely the cellular basis of distal airway remodeling in COPD.

Keywords: bronchiole; heterogeneity; remodeling; epithelium; regeneration

(Received in original form July 21, 2022; accepted in final form February 15, 2023)

*Co-first authors.

Supported by NIH grants U01 HL145561, R01 HL123544, and R01 HL127393 (to R.S.). We thank personnel of the Marsico Lung Institute Tissue Procurement and Cell Culture Core (supported by Cystic Fibrosis Foundation grant BOUCHE19R0 and NIH grant DK065988) for providing lung tissue samples. S.B.M. was supported by the American Lung Association Senior Research Training Fellowship and the Weill Cornell Clinical and Translational Science Center TL1 Training Award. A.F.R. was supported by National Cancer Institute grant T32 CA203702. B.R. was supported by U.S. Department of Veterans Affairs career development grant IK2BX003841. T.S.B. was supported by the U.S. Department of Veterans Affairs Merit Review Grant 2 I01 BX002378.

Author Contributions: R.S. conceived, supervised, and supported the study; S.R. and S.B.M. established the methodology of lung tissue dissection, processing, and cell isolation; S.R. performed tissue dissection, immunostaining and analysis, and *in vitro* studies; S.R., A.F.R., and R.S. performed analysis of immunostaining and imaging data; Y.H. performed analysis of RNA-sequencing (RNA-seq) and single-cell RNA-sequencing data; H.R. participated in imaging mass cytometry analysis; O.E. supervised analysis of RNA-seq, single-cell RNA-seq, and imaging CyTOF data; S.H.R., B.R., V.P., J.A.K., T.S.B., F.D'O., and N.K.A. provided lung tissue samples; A.U. assisted with lung tissue procurement; S.H.R., V.P., and T.S.B. provided histological samples for imaging studies; F.J.M. assisted with clinical expertise and resources; S.R., Y.H., O.E., and R.S. performed integrated data analysis and interpretation of data; R.S. wrote the manuscript. All authors reviewed and edited the final version of the manuscript.

Correspondence and requests for reprints should be addressed to Renat Shaykhiev, M.D., Ph.D., Department of Medicine, Weill Cornell Medical College, Room A-342, 1300 York Avenue, New York, NY 10021. E-mail: res2003@med.cornell.edu.

Am J Respir Crit Care Med Vol 207, Iss 9, pp 1171–1182, May 1, 2023

Copyright © 2023 by the American Thoracic Society

Originally Published in Press as DOI: 10.1164/rccm.202207-1384OC on February 16, 2023

Internet address: www.atsjournals.org

At a Glance Commentary

Scientific Knowledge on the

Subject: Accumulating evidence suggests that distal conducting airways, including preterminal and terminal bronchioles (pre-TBs/TBs), represent the primary site of structural alterations that underlie airflow limitation in chronic obstructive pulmonary disease (COPD). The cellular basis of these alterations remains unclear, in part because of poor accessibility of pre-TBs/TBs and limited knowledge about their cellular organization and homeostasis.

What This Study Adds to the

Field: In this study, using a novel airway dissection method, we isolated and characterized, at single-cell resolution, the region-specific cellular ecosystem of human distal airways. This analysis identified terminal airway-enriched secretory cells (TASCs), a unique epithelial cell population of distal airways, enriched in TBs and expressing an intermediate molecular pattern associated with the transition of distal conducting airways to the respiratory zone. TASCs were lost in pre-TBs/TBs in COPD paralleled by changes in the microenvironment, including increased frequency of CD8⁺ T cells and augmented IFN- γ signaling, which suppressed the regenerative potential of distal airway epithelial progenitors. Thus, altered maintenance of the unique cellular organization of pre-TBs/TBs represents the key biological manifestation and likely the cellular basis of distal airway pathology in COPD.

Distal conducting airways, including preterminal and terminal bronchioles (pre-TBs and TBs, respectively), connect more proximal segments of the tracheobronchial tree with the alveolar zone of the lung, where gas exchange takes place

(1). Distally, TBs open to respiratory bronchioles (RBs), transitional segments, which lead to alveolar ducts and alveoli (1). The TB–RB transition occurs within the secondary pulmonary lobules (“lobules”), structural and functional lung tissue units, supplied by pre-TBs (2, 3). Recent imaging studies show that remodeling and loss of bronchioles along the pre-TB–RB continuum underlie progressive airflow limitation in chronic obstructive pulmonary disease (COPD) (4–11), the third leading cause of death worldwide (12). The cellular basis of these alterations remains poorly understood, in part because of poor accessibility of pre-TBs/TBs and limited knowledge about their cellular organization and homeostasis.

To address this problem, in this study, we established a novel distal airway dissection approach, which regards pre-TBs, the last macroscopically visible segments along the bronchial pathway (2), as anatomical landmarks for isolation of prelobular distal conducting airways and lobules containing TBs and associated respiratory segments, facilitating characterization of their cellular organization at single-cell resolution. Using this approach, we identified terminal airway-enriched secretory cells (TASCs), a unique epithelial cell population of distal airways, enriched in TBs, particularly at TB–RB junctions, and exhibiting an intermediate molecular phenotype associated with transition of distal conducting airways to the respiratory zone. A marked loss of TASCs was observed in pre-TBs/TBs in COPD, accompanied by changes in the composition of region-specific vascular and immune microenvironments in these bronchioles, suggesting that altered maintenance of the unique cellular architecture of pre-TBs/TBs underlies distal airway remodeling in COPD. Some of the results of these studies have been reported previously in the form of a preprint (13).

Methods

Lung tissue samples from 44 normal lung donors and 18 subjects with COPD were obtained from the University of North Carolina Tissue and Cell Culture Procurement Core, Columbia University Medical Center Lung Transplant Program,

Vanderbilt University Medical Center, and Weill Cornell Medicine Thoracic Surgery Biobank using protocols approved by the respective institutional review boards. Additional lung tissue samples from four healthy lung donors and three subjects with COPD were obtained from US Biomax and the National Institutes of Health/National Heart, Lung, and Blood Institute Lung Tissue Research Consortium for imaging studies. Sample details are provided in Tables E1–E3 in the online supplement.

For single-cell RNA sequencing (scRNA-seq) and *in vitro* studies, cells were isolated from proximal (P) airways (bronchi, generations 1–4), preterminal (pre-T) airways (pre-TBs and generations 3–4 proximal to pre-TBs; luminal diameter <2 mm), and terminal (T) airway region (containing TBs and descending respiratory segments within the lobule) dissected from a subset of lung tissue samples (Tables E1 and E3) using a region-precise dissection method described in the RESULTS section and detailed in the online supplement (Figure E1 in the online supplement). scRNA-seq (10 \times Genomics) data were processed and analyzed using Seurat version 4 (14), doublets were detected by DoubletFinder (15) and removed, and cell clusters were annotated on the basis of marker genes as detailed in the online supplement (Figure E2).

Immunofluorescence (IF) analysis of lung tissue samples was performed as previously described (16–18). Imaging cytometry by time of flight (CyTOF) was performed using the Hyperion (Fluidigm) system as described in the online supplement. Samples used in imaging analyses are described in Table E2. In *in vitro* studies, basal cells (BCs) isolated from different airway regions (Table E3) were cultured in the air–liquid interface (ALI) system to induce their differentiation, which was evaluated by bulk RNA-seq and scRNA-seq, TaqMan real-time PCR, and IF analysis as detailed in the online supplement.

Results

Anatomical Landmarking of Human Distal Airways

On the basis of the anatomical definition of pre-TBs as the last macroscopically

This article has a related editorial.

This article has an online supplement, which is accessible from this issue's table of contents at www.atsjournals.org.

recognizable segments along the bronchial pathway that supply the lobule (2, 3), we developed a distal airway dissection approach that regards pre-TBs as the boundary between preterminal (pre-T; pre-TBs and three or four generations proximal to pre-TBs) and terminal (T; intralobular segments from TBs to alveoli) airway-enriched regions (Figures 1A and E1). Large cartilaginous bronchi represented proximal (P) airways (Figures 1B and E1). The natural distribution of all major tissue elements, including the airway surface epithelium (ASE), stroma with smooth muscle (SM) and vessels, and region-specific histological landmarks, such as cartilage and submucosal glands (SMGs) in P-airways, alveolar attachments in pre-T/T regions, and TBs, RBs, alveolar ducts, and alveoli in the T region, was preserved in isolated samples (Figures 1B and E1).

Cellular Diversity along the Proximal–Distal Airway Axis

Transcriptomes of 111,412 single cells isolated from P airways of 5 normal lung donors, pre-T airways of 12 normal lungs and 5 subjects with COPD, and T region from 7 healthy lungs were captured by scRNA-seq. Uniform Manifold Approximation and Projection clustering identified 48 cell types/subtypes (Figures 1C and E2; details in the online supplement), which were classified by hierarchical clustering into three superfamilies: 1) epithelial (including ASE, SMG, and alveolar families), 2) structural (stromal and endothelial [En] families), and 3) immune (myeloid and lymphoid families) (Figure 1D). Selected markers of the identified cell groups are shown in Figures 1E and E2 (complete marker gene lists are provided in Table E4).

Epithelial. The ASE family included BCs, intermediate cells (ICs; *SERPINB3^{high}*), and previously described differentiated cell populations, such as secretory (S, including common [S1, *SCGB1A1^{high}*] and mucus-producing [S-Muc]), ciliated (C, including common [C1] and serum

amyloid A [SAA] gene-expressing [C-s] [19]), S-C-intermediate cells (deuterosomal pre-C cells [p-C] and hybrid cells sharing C- and S-markers [20–22]), ionocytes (23, 24), and neuroendocrine cells. The SMG family included mucous (G-Muc), serous (G-Ser), and myoepithelial cells. The alveolar type (AT) family included alveolar type 1 (AT1) and 2 (AT2) cells. A “bridge” cluster was identified between S cells and AT2 cells (Figure 1C). Cells in this cluster were marked by expression of *SCGB3A2* and *SFTPB*, identified in our previous study as distal airway epithelial signature genes (16) and present almost exclusively in pre-T/T airways. Therefore, we termed these cells “terminal airway-enriched secretory cells,” or TASCs.

Structural. Stromal cells included chondrocytes (*SNORC*), fibroblasts (including common [Fb1], *CCL19⁺* [Fb2 including *SFRP2⁺* Fbs (25)], matrix (Fb3, *ELN*, *COL1A1*, including *ACTA2⁺* myoFbs), and Fb4 containing *GPC3⁺* *FGFR4⁺* alveolar Fbs (25), SM cells (SM1 and SM2 expressing vascular SM markers *ADIRF*, *NOTCH3*, *PDGFRB*, and SM3 expressing airway SM markers *DES* and *CNN1* (25)). Cells expressing markers of neuronal and glial/Schwann cells (Gli; *CDH19*, *MPZ*, *NRXN1*) were also identified. En cells included arterial (En-a), common capillary (En-c1), cells expressing markers of alveolar capillary aerocytes (25) (En-ca), venous (En-v, including cells expressing fenestrated En-c markers *ACKR1* and *PLVAP* [25]), En-sm coexpressing En and SM markers, and lymphatic (En-l).

Immune. Myeloid cells included neutrophils, mast cells, monocytes, macrophages (inflammatory [M1; *SPP1*, *CCL3*], noninflammatory [M2; *MSR1*, *CCL18*], and M1–2 mixed), and dendritic cells (conventional and plasmacytoid). Lymphoid cells included B, plasma, T, and natural killer (NK) cells. T cells included cells expressing markers of central and naive T cells (Tcn; *CCR7*, *IL7R*) (22), T-*ifn* expressing IFN response genes, CD8-enriched (including resident memory

[Trm; *CXCR6*, *CCL5*] (26–28) and remaining [CD8⁺-T1]), and T cells expressing NK cell markers (T-NK).

Regional Heterogeneity of Epithelial Cells

SMG cells were enriched in P airways, and AT cells were found only in pre-T/T regions (Figure 2A). Among ASE cells, ICs were enriched in P airways, whereas the overall frequency of S-C-intermediate cells was higher in pre-T/T airways (Figures 2A and 2B). Although the overall frequency of S cells was comparable in all regions, TASCs were found almost exclusively in pre-T/T regions, with significant enrichment in the T region (Figure 2B; Table E5). TASCs exhibited a transitional molecular pattern integrating features of S and AT2 cells. Unlike other S cells, TASCs expressed *SCGB3A2*, *SFTPB*, and genes also expressed in AT cells (*RNASE1*, *SFTPA2*, *HOPX*, *SFTPA1*). Compared with AT2 cells, TASCs expressed S cell genes *SCGB1A1* and *SCGB3A1* but showed significantly lower expression of AT2 markers *SFTPC*, *SFTPA1*, and *SFTPA2*. Notably, *SCGB3A2* and *MGP* were expressed in TASCs at higher levels than in both S and AT2 cells (Figures 2C and 2D; Table E6). No cell population analogous to TASCs was found by analyzing scRNA-seq datasets of the mouse lung (29, 30), where *Scgb3a2* was broadly expressed in *Scgb1a1⁺* S cells and *Sftpb* expression was largely restricted to AT2 cells (Figure E2Y₄).

Morphologically, TASCs represented lumen-facing nonciliated airway epithelial cells that contained SFTPB and/or SCGB3A2 proteins typically accumulated in secretory granules in their apical cytoplasmic domain and occasionally released into airway lumen (Figures 2E, 2F, and E4). SCGB3A2⁺ TASCs constituted 8% and 23% of epithelial cells in pre-TBs and TBs, respectively, and >40% of cells in simple columnar-to-cuboidal epithelium at TB–RB junctions (Figure 2G). SFTPB marked a broader subset of TASCs (16% of ASE cells in pre-TBs, 33% in TBs, and 54% at TB–RB junctions; Figure 2H). In pre-TBs and proximal aspects of TBs, TASCs

Figure 1. (Continued). (B) Examples of hematoxylin and eosin staining of dissected P, pre-T, and T regions. Histological landmarks are shown. (C) Uniform Manifold Approximation and Projection (UMAP) clustering of 111,744 single cells isolated from P (*n* = 5), pre-T (*n* = 13), and T (*n* = 7) regions of healthy lungs and pre-T airways of subjects with COPD (*n* = 5). (D) Dendrograms based on hierarchical clustering of cell groups identified in C based on top 2,000 variable genes using Spearman correlation and complete linkage algorithm. Specific cell groups within epithelial, structural, and immune superfamilies are shown. (E) Dot plots showing expression of selected marker genes in indicated cell groups. Dot size reflects percentage of cells within a group expressing a given gene. Dot color shows mean expression level as indicated.

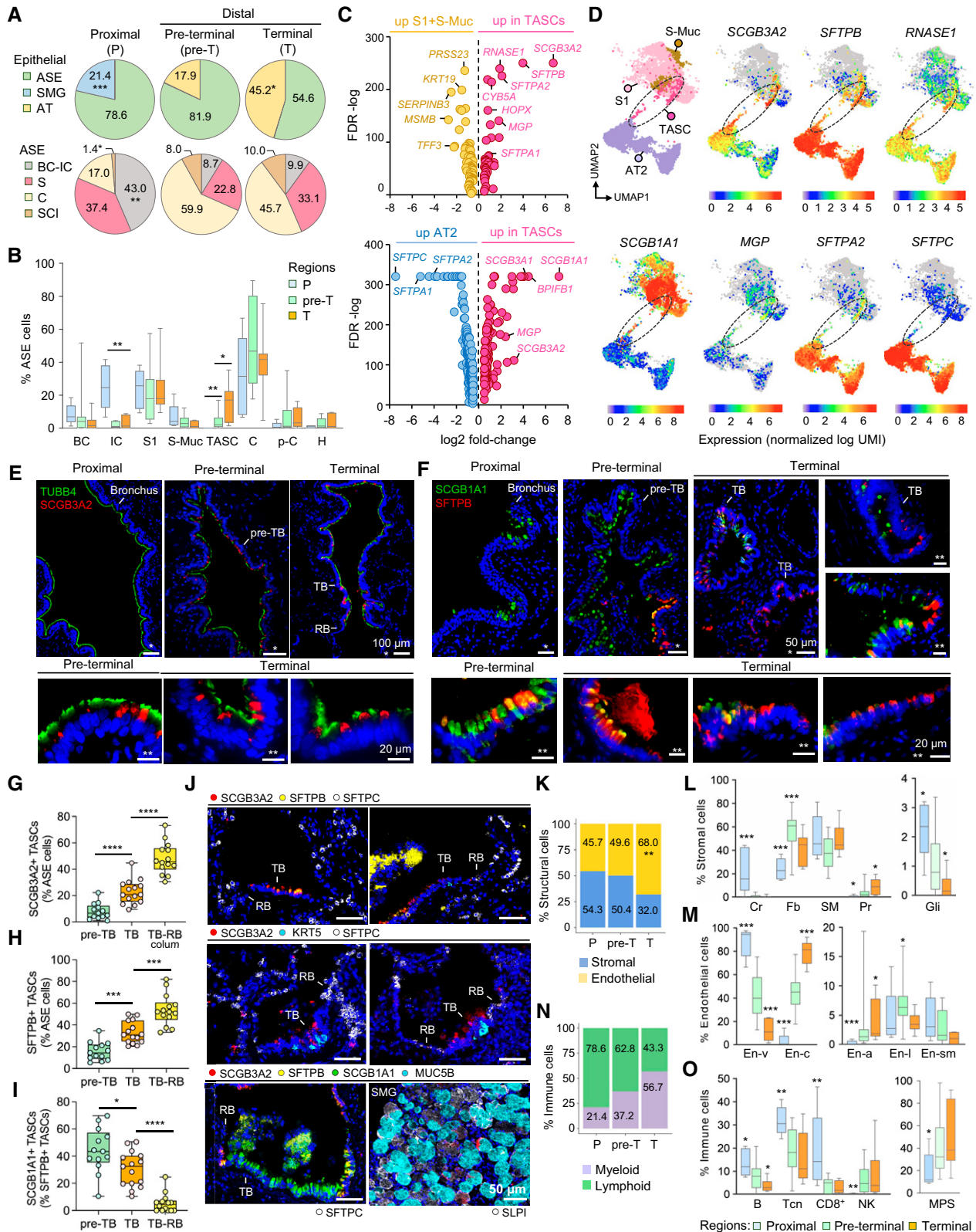


Figure 2. Region-specific cellular heterogeneity along the bronchoalveolar axis. (A) Proportions (percentages) of cells belonging to indicated families within epithelial superfamily (upper; airway surface epithelium [ASE]; SMG; alveolar epithelium); average percentage of cells per sample in indicated regions of normal lungs and in ASE family as described in Figure 1D. (B) Average percentage of cells belonging to indicated cell types (per sample as described in A) within ASE in different regions. (C) Volcano plots (based on single-cell RNA-sequencing data) showing

had a dome-shaped appearance, resembling typical club cells (31), whereas, at TB–RB junctions, they acquired a cuboidal shape typical for transitional epithelium of RBs (32) (Figures E4A and E4B).

The molecular pattern of TASCs changed along the pre-TB–RB continuum: 44.2% of TASCs in pre-TBs coexpressed SCGB1A1 protein, a marker of common S cells, compared with 30.5% of TASCs in TBs and only 5.5% at TB–RB junctions (Figure 2I). In the T region, TASCs had higher expression of *SFTPA2* than those in pre-T airways (Figure E5). In contrast to AT2 cells, TASCs were typically SFTPC-negative (Figure 2J). As reported earlier (33), a subset of serous SMG cells were SCGB3A2⁺, but they did not express *SFTPB* or *SCGB1A1* (Figure 2J) and, based on their transcriptomic profiles, clustered separately from TASCs (Figure 1C).

Regional Heterogeneity of Structural and Immune Cells

En cells were most abundant in the T region (Figure 2K). Chondrocytes were found in cartilaginous P airways (Figure 2L). Among fibroblasts, Fb2 were most frequent in P airways, whereas Fb3 and Fb4 increased in frequency along the proximal–distal axis, as did pericytes (Table E5). The frequency of Gli cells declined along this axis (Figure 2L). Among En cells, capillary En cells were enriched in the T region, and venous/fenestrated En cells were highest in P airways, whereas lymphatic En cells were most abundant in the pre-T region (Figure 2M). Among immune cells, myeloid and lymphoid cells showed reciprocal enrichment along the proximal–distal axis, with an overall higher proportion of lymphoid cells (e.g., B-, Tcn-, and CD8⁺ T cells) in P airways and an overall higher frequency of the mononuclear phagocyte

system cells in pre-T/T regions (Figures 2N and 2O; Table E5).

Altered Cellular Composition of Distal Airways in COPD

Comparison of pre-T airways from 5 subjects with COPD and 12 healthy lung donors in our scRNA-seq analysis identified that disease-related changes preferentially involved cell groups contributing to regional heterogeneity along the proximal–distal airway axis. This included loss of TASCs and En-c cells normally enriched in pre-T/T regions and increased proportions of Gli and CD8-T1 cells normally enriched in P airways, accompanied by a marked increase in mast cell frequency in COPD versus normal pre-T airways (Figures 3A and 3B). Notably, CD8⁺ T cell frequency was also significantly increased in pre-TBs of nondiseased smokers versus nonsmokers (Figure 3B), paralleled by an increased proportion of BCs in the pre-TB epithelium, suggestive of smoking-induced BC hyperplasia, but without changes in the distribution of other epithelial cell populations, including TASCs (Table E5).

Changes in the cellular composition of COPD pre-TBs were accompanied by the altered gene expression in individual cell types, with the highest number of upregulated genes observed in mast cells, BCs, Fb1, CD8-T1, Gli, M2, and T-NK and the highest numbers of suppressed genes in En-ca, TASCs, and S1 cells (Figure 3C; Table E7). Among the genes downregulated in the ASE of COPD pre-T airways were, as expected, TASC markers *SCGB3A2* and *SFTPB* and common S cell genes *SCGB1A1* and *SCGB3A1* also expressed by TASCs (Figure 3D; Table E8). The IFN- γ signaling pathway, including IFN- γ response genes, was enriched among the genes upregulated

in the ASE of COPD versus normal pre-T airways (Figure 3E; Table E9).

IF analysis, in which >130,000 cells lining pre-TBs/TBs in 11 COPD and 24 normal lungs were captured (Figure 3F; Table E2), revealed a dramatic loss of SCGB3A2⁺ and SFTPB⁺ TASCs in pre-TBs and TBs of patients with COPD compared with nondiseased lungs (Figures 3F and 3G). SFTPB⁺ TASCs were found in all pre-TBs in nondiseased lungs, and SCGB3A2⁺ TASCs were found in >90% of them, whereas no TASCs could be found in 55.4% and 10.9% of pre-TBs in subjects with COPD, based on SCGB3A2 and SFTPB positivity, respectively (Figure 3G). Whereas SCGB3A2⁺ TASCs were detected in >99% of TBs in healthy lung donors, these cells were absent in 26.9% of TBs in subjects with COPD (Figure 3G). Remarkable heterogeneity was noted with regard to the extent of TASC loss in different patients with COPD and in different pre-TBs/TBs (Figures 3F–3H).

Notably, SCGB1A1⁺ S cells were preserved in COPD pre-TBs/TBs, where TASCs were absent (Figures 3H and E6B). Consistent with this, no significant difference was found in the frequency of SCGB1A1⁺ S1 cells in pre-TBs/TBs of COPD versus normal lung donors, and there was no correlation between TASC loss and changes in SCGB1A1⁺ S1 cell frequency in pre-TBs/TBs (Figure E7). No significant change was detected in the TASC frequency in pre-TBs/TBs of nondiseased smokers versus nonsmokers (Figure E8).

In agreement with scRNA-seq data, imaging CyTOF determined an increased density of CD8⁺ cells, including intraepithelial CD8⁺ cells, in pre-TBs/TBs in COPD versus normal lung donors (Figures 3I, 3J, and E10A). A particularly high density of total and intraepithelial CD8⁺ cells was detected in COPD pre-TBs/TBs with a lower

Figure 2. (Continued). differentially expressed genes (DEGs) identified by comparing all (upper) terminal airway-enriched secretory cells (TASCs) and other S (S1 and S-Muc) cells and (lower) TASCs and alveolar type 2 (AT2) cells. DEGs shown with false discovery rate <0.01 and log₂ fold change greater than 0.5 or less than -0.5. (D) Portion of the Uniform Manifold Approximation and Projection (UMAP) graph shown in Figure 1C. A clustering region where TASCs form a bridge between S and AT2 cells is demarcated (dashed line). Expression of selected DEGs identified in the analysis shown in C is color mapped. (E, F) Immunofluorescence (IF) images showing expression of (E) SCGB3A2 and tubulin β 4 (TUBB4; cilia marker) and (F) SFTPB and SCGB1A1 (S1 cell marker) in indicated regions. (G–I) Percentage of (G) SCGB3A2⁺ TASCs, (H) SFTPB⁺ TASCs among ASE cells, and (I) SCGB1A1⁺ cells among SFTPB⁺ TASCs in indicated regions. TB-RB, simple epithelium (column, columnar) in TB–RB transition areas. (J) Representative CyTOF images showing expression of indicated markers in different regions. (K) Proportions of structural cell families (average percentage of cells per sample) in different regions. (L, M) Average percentage of indicated cell types (per sample; as described in A; cell type names as described in Figure 1D) within stromal (L) and endothelial (En; M) cell families. (N) Proportions of cells representing immune families (average percentage of cells per sample) in different regions. (O) Average percentage of indicated cell types (per sample; as described in A; cell type names as described in Figure 1D) in different regions. (A, B, G–I, K–O) **P* < 0.05, ***P* < 0.01, ****P* < 0.005, and *****P* < 0.0001 (two-tailed Mann-Whitney test) versus other or indicated regions. CyTOF = cytometry by time of flight; RBs = respiratory bronchioles; SMG = submucosal gland; TB = terminal bronchioles.

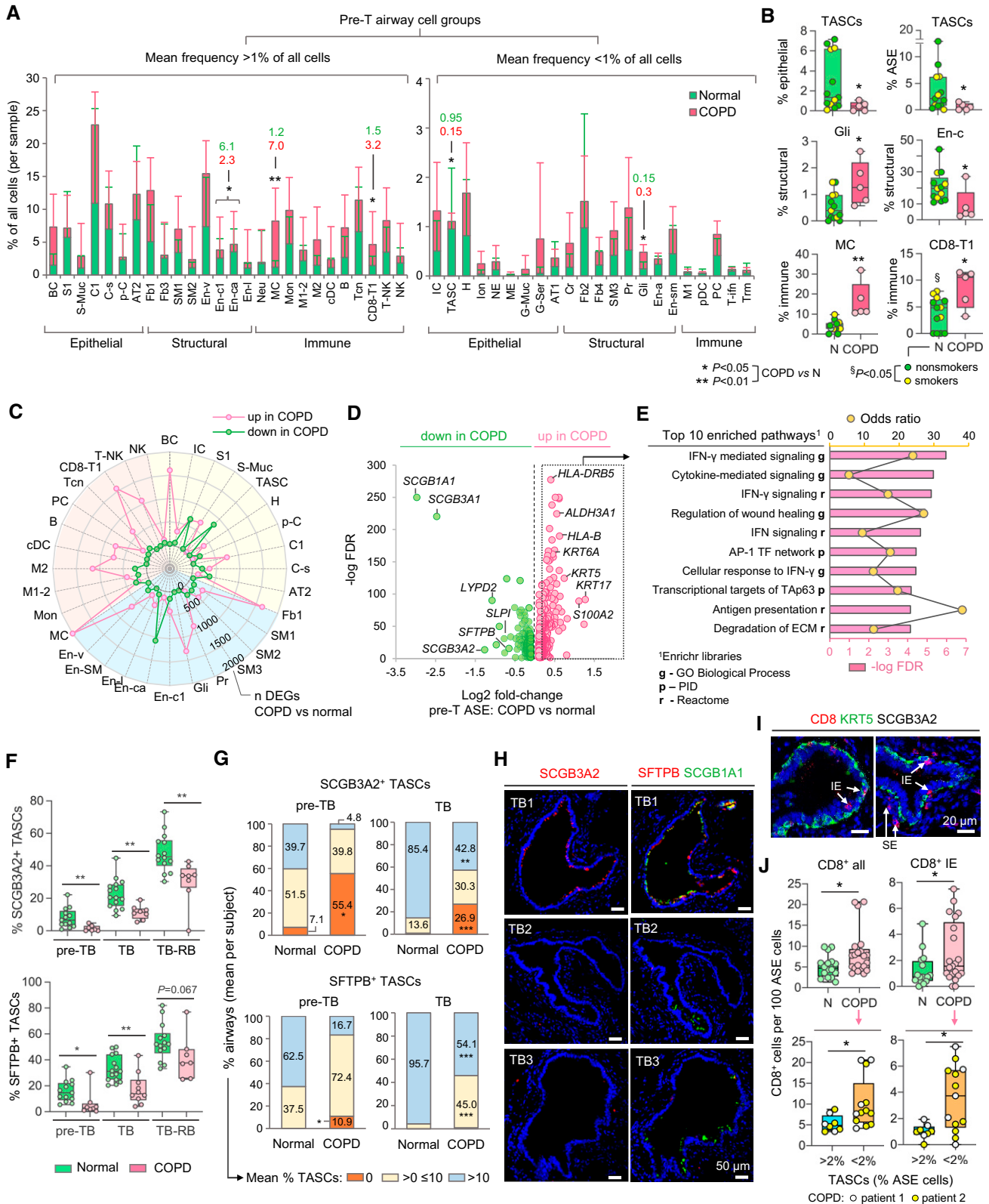


Figure 3. Changes in cellular organization of chronic obstructive pulmonary disease (COPD) distal airways. (A, B) Proportions (percentages) of indicated cell groups (single-cell RNA-sequencing [scRNA-seq] data; abbreviations described in Figure 1D) in pre-terminal (pre-T) airway samples of donors without lung disease (normal; $n=13$) and subjects with COPD ($n=5$): (A) Mean percentage of cells in indicated cell groups among all cells per sample (values are shown for cell groups with significant differences between the groups). Error bars represent

TASC frequency (<2% of ASE cells) (Figure 3J; Table E3).

Distal Airway BCs Are a Cellular Origin of TASCs

To identify the cellular origins of epithelial heterogeneity along the proximal–distal airway axis, we isolated BCs, ASE stem cells (34, 35), from P and distal (D; pre-T) airways of six normal lung donors and assessed their differentiation in an ALI model (Figure 4A; Table E3). RNA-seq analysis of epithelia generated by P and D airway BCs identified 2,005 differentially expressed genes (Table E11). Among genes robustly upregulated in D airway BC-derived epithelia, ~21% were TASC marker genes (e.g., *SFTPB*, *SCGB3A2*, *SFTA2*, *RNASE1*, and *SFTPA2*) (Figures 4B and 4C). *SCGB3A2*⁺ cells were uniquely present in epithelia derived from D airway BCs, whereas *Muc5AC*⁺ S cells were more frequent in P airway BC-derived epithelia (Figure 4D).

To evaluate distal airway epithelial differentiation at single-cell resolution, D-airway BC-derived epithelia at different time points of ALI culture were profiled using scRNA-seq. A total of 36,321 cells were captured in this analysis (Table E12). The initial (ALI day 0; d0) epithelia included two BC subsets, typical and S-like (BC-s). At d3, *SERPIN3*^{high} ICs, squamous (*KRT6A*, *SPRR1B*), p-C, initial C cells, ionocytes, and tuft-like cells emerged (Figures 4E, 4F, and E9). At d7, S cells emerged (56% of cells), and TASCs appeared as an extension of the S cell cluster. By d28, TASC frequency reached 30%, and the overall composition of the

epithelium resembled that of pre-T airways *in vivo*, with the differentiated cell types constituting together >80% of ASE cells (Figures 4E and 4F; Table E12).

Marker profiles of cell types generated by D-airway BCs *in vitro* (Table E13) were similar to those *in vivo*. The highest degree of similarity was observed for C1 cells (>90% overlap of *in vitro* and *in vivo* markers) followed by C-s (56.4%), p-C (48.8%), BCs (47.0%), ICs (38.9%), TASCs (35.9%), and ionocytes (28%) (Figure 4G; Table E14). Compared with S1 cells derived in the same culture, TASCs showed upregulation of 84 genes, 40 of which were among those identified in a similar comparison *in vivo*, including *SCGB3A2* and *SFTPB* (Figure 4H; Table E15). Thus, distal airway BCs represent region-specific progenitors regenerating TASCs.

IFN- γ Inhibits TASC Regeneration by Distal Airway BCs

On the basis of our findings of increased IFN- γ signaling in COPD pre-TB ASE and increased density of CD8⁺ T cells, a major *IFNG*-expressing cell population, in COPD pre-TBs/TBs with low TASC frequency, we hypothesized that TASC loss in COPD could be mediated by IFN- γ signaling in D-airway BCs. In support of this hypothesis, in COPD pre-TBs/TBs, CD8⁺ T cells were found in close proximity to BCs (Figure 3I), and the latter expressed IFN- γ receptor genes (Figure E10C). Exposure of D-airway BCs to IFN- γ during their differentiation in the ALI model induced IFN- γ response genes (*MX1*, *IFIT1*, *CXCL10*) and suppressed

TASC marker genes *SCGB3A2* and *SFTPB* (Figures 4I and E10D_{1–2}) accompanied by broad transcriptional changes (Table E16). Genes up- and downregulated by IFN- γ in this analysis overlapped with 12.6% and 27.8% of differentially expressed genes having the same direction of change in the ASE of COPD versus normal pre-TBs (Figure E10D₃).

IF analysis identified reduced frequency of *SFTPB*⁺ TASCs paralleled by loss of *SCGB1A1*^{high} S cells and ciliated cells and increased proportion of *KRT6*⁺ ICs in IFN- γ -treated ALI epithelia, without consistent changes in *KRT5*⁺ BCs/ICs and *MUC5AC*⁺ mucus-producing cells (Figures 4J and E10D_{4–6}; Table E17). Notably, increased expression of *KRT6A* was also observed in the pre-TB ASE of patients with COPD (Figure 3D). Thus, IFN- γ suppresses TASC regeneration by inhibiting the normal differentiation potential of distal airway BCs.

Discussion

In this study, using a novel, anatomical landmark–based distal airway dissection method, we characterized, at single-cell resolution, the unique cellular composition of human distal airways. This method allowed us to capture the entire continuum of small airways undergoing structural and functional alterations in COPD (4–11) and to identify, for the first time, biological changes occurring in these airways in COPD at single-cell resolution.

Figure 3. (Continued). standard deviation. (B) Mean percentage of cells in indicated cell groups among all cells per sample within superfamilies (dots: individual samples). (C) Radar plot showing numbers of differentially expressed genes (DEGs) identified by comparing scRNA-seq average gene expression profiles of indicated cell groups in pre-T samples (COPD vs. normal) described in A. Criteria for cell types/subtype inclusion: >10 cells in each group (normal; COPD); at least 3 cells in >50% samples in each group. Colored areas: epithelial (yellow), structural (blue), and immune (red) superfamilies. Dots show numbers of DEGs up- or downregulated in COPD versus normal samples (Mann-Whitney $P < 0.05$). (D) Volcano plot showing DEGs (false discovery rate <0.05) identified by comparison of scRNA-seq average expression profiles of airway surface epithelial (ASE) cells in COPD versus normal pre-T samples described in A. (E) Top 10 annotation categories among Gene Ontology (GO) Biological Process; Reactome and NCI-Nature Pathway Interaction database (PID) libraries enriched among DEGs upregulated in ASE of COPD versus normal pre-T samples (\log_2 fold change >0.2); ranked by $-\log$ false discovery rate of enrichment; based on Enrichr analysis. (F–H) Immunofluorescence analysis. (F) Mean percentage of *SCGB3A2*⁺ (upper) and *SFTPB*⁺ (lower) terminal airway-enriched secretory cells (TASCs) per subject among ASE cells in preterminal bronchiole (pre-TB), TB, and TB-RB (defined as in Figures 2G–2I) of healthy lung donors and subjects with COPD. Dots represent individual subjects (see Table E2 for details). (G) Distribution of distal airways (pre-TBs and TBs) in healthy and COPD lung tissue samples (described in F) based on average percentage of *SCGB3A2*⁺ (upper) and *SFTPB*⁺ (lower) cells in the ASE (per subject). (H) Representative immunofluorescence images showing *SCGB3A2*⁺ TASCs, *SFTPB*⁺ TASCs, and *SCGB1A1* expression in different TBs of the same COPD patient's lung. (I, J) Imaging CyTOF. (I) Representative images showing CD8⁺ cells (intraepithelial [IE]; subepithelial [SE]) in distal airways (pre-TBs/TBs) of patients with COPD; *KRT5*, keratin 5; *SCGB3A2* (white). (J) Frequency of all (left) and IE (right) CD8⁺ cells in distal airways of normal (N; $n = 3$; 16 airways) and COPD ($n = 2$; 21 airways) subjects (upper panel); shown separately in the lower panel for COPD distal airways with TASC frequency: >2% and <2% of epithelial cells. * $P < 0.05$, ** $P < 0.01$, *** $P < 0.005$ (two-tailed Mann-Whitney test) COPD versus normal (A, B, F, G, and J, upper), and $^{\S}P < 0.05$ normal lung donors: smokers versus nonsmokers (two-tailed Mann-Whitney test) in B; COPD distal airways with TASC frequency >2% versus <2% of epithelial cells (J, lower). CyTOF = cytometry by time of flight; RB = respiratory bronchioles.

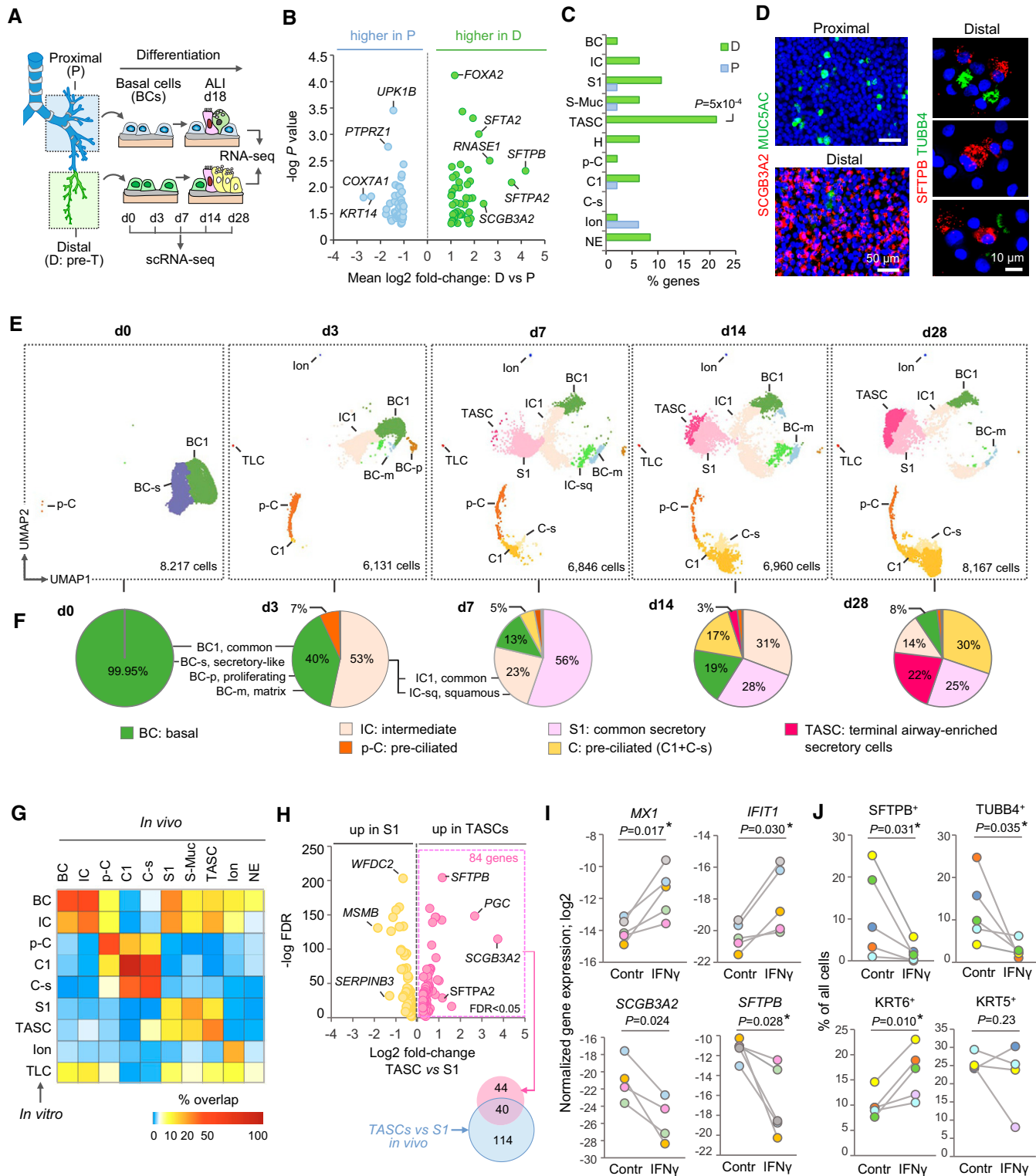


Figure 4. Distal airway basal cells (BCs) as the cellular origin of terminal airway-enriched secretory cells (TASCs). (A) Design of *in vitro* studies. BCs isolated from proximal (P) and distal (D; pre-terminal [pre-T]) airways were cultured under the same conditions in the Transwell system. After BCs established a confluent layer, apical medium was removed to establish an air-liquid interface (ALI), and medium was supplied from the basolateral side. Samples were analyzed at indicated ALI time points representing different stages of BC differentiation. (B) Volcano plot: Differentially expressed genes (DEGs) identified by comparison of ALI day 18 epithelia generated by BCs from P and D airways of six normal lung donors (shown DEGs with \log_2 fold change >1 and two-tailed paired *t* test; $P < 0.05$). (C) Proportions (percentages) of DEGs upregulated

Region-precise approach in our study allowed us to identify TASCs, a unique secretory cell population of distal airways enriched in TBs and exhibiting an intermediate molecular pattern, including SCGB3A2 and SFTPB, associated with the transition of distal conducting airways to the respiratory zone. Contributing to this transition, TASCs gradually changed their phenotype along this continuum from SCGB1A1-expressing columnar cells resembling classical club cells (31) in pre-TBs and proximal parts of TBs to SCGB1A1-negative cuboidal cells at TB–RB junctions that acquire *SFTPA1* expression, which marks the entrance to the respiratory zone (32). No TASC analog could be found in mouse lung scRNA-seq datasets (29, 30), consistent with the absence of RBs and, thus, lack of TB–RB transitional zone, in the murine lungs (36, 37).

In our earlier study (16), TASC marker genes *SCGB3A2* and *SFTPB* were identified among distal airway epithelial signature genes (i.e., those whose expression was enriched in the epithelia obtained by bronchoscopy from small airways; 10th–12th generation) and mapped to distal airway S cells. Thus, although TASCs are enriched in TBs, the initial acquisition of the molecular state characteristic of TASCs begins in more proximal airways, suggesting that a gradient of secretory cell specialization exists along the proximal–distal airway axis. Since our original identification of SCGB3A2⁺ SFTPB⁺ distal airway-specific S cells (16), which we now define at single-cell resolution as TASCs, similar cell populations, including SCGB3A2⁺ SFTPB⁺ SCGB1A1⁺ pre-TB S cells and SCGB3A2⁺ SFTPB⁺ SCGB1A1[−] TB–RB S cells (TRB-SCs) (38) and “respiratory airway secretory” (RAS) cells (37) have been found. On the basis of their molecular profiles and anatomical distribution, these cell

populations likely represent distinct intermediate states of TASCs along the pre-TB–RB continuum, with pre-TB S cells being SCGB1A1⁺ club cell-like TASCs in pre-TBs and proximal aspects of TBs, whereas TRB-SCs and RAS cells representing SCGB1A1[−] cuboidal TASCs at TB–RB junctions.

Consistent with the nature of TASCs as S cells of distal conducting airways, our study identified that BCs residing in pre-TBs/TBs harbor an intrinsic “regional memory” allowing these progenitors, but not their proximal airway counterparts, to generate TASCs *in vitro*. This finding supports the concept of region-specific differentiation potential of airway BCs (16, 38–40). By contrast, despite their molecular similarity to TASCs, TRB-SCs and RAS cells have been shown to originate from an alveolar progenitor or serve as alveolar progenitors themselves, respectively (37, 38). It is possible that these cells represent a subset of TASCs located in the most distal aspects of TB–RB junctions and RBs, where BCs are absent, and therefore their maintenance likely relies on BC-independent regenerative mechanisms unique to this transitional region.

Enrichment of TASCs in pre-TBs/TBs was accompanied by changes in the distribution of nonepithelial cell populations contributing to region-specific cellular ecosystems. This included a progressive increase in the frequency of capillary En-cells paralleled by loss of venous En-cells with molecular features of fenestrated endothelium (25, 41, 42) along the proximal–distal airway axis. Schwann cells, glial representatives in the peripheral nervous system (43), were captured in our study as a proximal airway-enriched cell type. Lymphoid cells (e.g., B cells and various T cell subsets), including CD8⁺ T cells, were more abundant in proximal airways, whereas cells of the mononuclear phagocyte system

were more frequent in the distal region, suggesting that homeostatic lung defense strategies are compartmentalized along the proximal–distal airway axis.

Many key aspects of region-specific cellular composition were altered in COPD distal airways. This included loss of TASCs in COPD pre-TBs/TBs, which was particularly dramatic in pre-TBs, where TASCs were about five times less frequent than in normal lungs. Loss of TASCs may have a significant impact on disease pathophysiology. As a major source of surfactants in distal airways, loss of TASCs may potentially lead to increased surface tension and collapse of these bronchioles during expiration and thus may contribute to small airway obstruction. Loss of TASCs at TB–RB junctions, where they compose up to 60–80% of epithelial cells and mediate the transition to the respiratory zone, could contribute to centrilobular emphysema, which develops in association with structural derangement of distal airways (5–7).

In our previous study (16), a downregulation of *SCGB3A2* and *SFTPB* and reduced SCGB3A2⁺ cell numbers were found in the small airway epithelium obtained by bronchoscopy from subjects with COPD and smokers without disease. Loss of TASCs in pre-TBs/TBs, however, was not observed in nondiseased smokers in the present study. This suggests that the pathologic process which leads to loss of TASCs in COPD may occur in a gradual manner, and molecular changes induced by smoking in more proximal airways may precede and predict loss of TASCs in pre-TBs/TBs as COPD develops. Although in our present study, it was not possible to obtain lung tissue samples from subjects with spirometrically defined mild/moderate COPD, this hypothesis can be addressed in longitudinal clinical studies that incorporate analysis of bronchoscopic samples from

Figure 4. (Continued). In ALI day 18 samples generated by BCs from matched P and D airways overlapping with marker genes of indicated pre-T airway surface epithelial (ASE) cell types based on single-cell RNA-sequencing analysis (criteria: log₂ fold change >1; false discovery rate [FDR] <0.05). (D) Immunofluorescence staining of the apical surface of ALI day 18 epithelia generated by BCs from P and D airways (left) and cytopreps of ALI day 17 epithelia generated by D airway BCs (right); blue: DAPI (nuclei). (E) Uniform Manifold Approximation and Projection (UMAP) clustering of cells at indicated time points of ALI culture of the same D airway BC sample; total number of single cells captured at each time point is indicated. (F) Percentage of cell types at ALI time points shown in E. TLCs, tuft-like cells. (G) Heatmap: Percentage of DEGs of indicated ASE cell types *in vivo* overlapping with those identified for cell types in ALI day 28 epithelia derived from D airway BCs shown in E using the same criteria: FDR <0.05; log₂ fold change >0.5 versus other ASE cells. (H) Volcano plot: DEGs (FDR <0.05) identified by comparison of TASCs and S1 cells in ALI day 28 epithelia generated by D airway BCs (shown in E); right side: overlap between DEGs upregulated in TASCs versus S1 *in vitro* and those identified in the same comparison *in vivo*. (I) Log₂ normalized expression of indicated genes detected by qPCR and (J) percentage of cells expressing indicated markers detected by immunofluorescence in ALI day 17–40 epithelia generated by D airway BCs in the absence (Contr) or presence of 5 ng/ml IFN-γ. Dot colors mark independent samples; P values based on paired *t* test (two-tailed in I; *Wilcoxon test <0.05 for *n* > 4 in I and J); see details in Figure E10D.

smokers without COPD and those with early disease.

Loss of TASCs in COPD distal airways was paralleled by a decreased frequency of capillary En-cells, including the En-ca subset exhibiting features of alveolar capillary aerocytes (25). Although aerocytes contribute to the alveolar–capillary interface (25, 42, 44), our data suggest that acquisition of the alveolar–capillary molecular phenotype occurs gradually and begins in distal pulmonary artery segments accompanying pre-TBs/TBs. These prealveolar capillaries may serve a region-specific niche supporting TASC maintenance in pre-TBs/TBs, and thus simultaneous loss of En-ca cells and TASCs in COPD pre-TBs could be related.

Furthermore, consistent with an earlier study (45), an increased frequency of CD8⁺ T cells was observed in COPD pre-TBs/TBs, accompanied by upregulation of the IFN- γ response program in the pre-TB epithelium. In COPD distal airways, CD8⁺ cells accumulated in close proximity to BCs and had particularly high density in pre-TBs/TBs

with the lowest TASC frequency. Notably, IFN- γ blocked the normal differentiation potential of pre-TB/TB BCs, including their ability to regenerate TASCs, suggesting that T cell–derived IFN- γ may mediate TASC loss in COPD. In concert with recent observations of increased IFN- γ expression in the areas of TB destruction in COPD (46), our findings further suggest that suppression of the regenerative potential of distal airway BCs by augmented IFN- γ signaling may underlie structural loss of pre-TBs/TBs in COPD (4–8). An increased CD8⁺ T cell frequency not accompanied by TASC loss was observed in our study in pre-TBs of smokers without disease. Thus, smoking-induced accumulation of CD8⁺ T cells in distal conducting airways may represent an early event during COPD development that precedes and likely mediates disease-associated changes in the distal airway epithelium.

Among other potential mechanisms of TASC loss and pre-TB/TB remodeling in COPD could be disease-related intrinsic changes in distal airway BCs compromising

their regenerative potential (47–49) or other alterations in COPD distal airway microenvironment identified in our study, including increased frequency of mast cells, known to infiltrate small airways in COPD (50), and Schwann cells, whose role in human lung pathophysiology is currently unknown.

Together, our study characterizes region-specific cellular organization of human distal airways and identifies its disarray, including loss of TASCs, a unique cell population of distal airway epithelium, as a major manifestation of small airway pathology in COPD at the cellular level. We believe that our study will provide the foundation for future investigations into mechanisms of COPD and other diseases affecting distal airways and that it will stimulate novel therapies aimed at the restoration of region-specific cellular organization of distal airways in lung disease. ■

Author disclosures are available with the text of this article at www.atsjournals.org.

References

- Haefeli-Bleuer B, Weibel ER. Morphometry of the human pulmonary acinus. *Anat Rec* 1988;220:401–414.
- Reid L. The secondary lobule in the adult human lung, with special reference to its appearance in bronchograms. *Thorax* 1958;13:110–115.
- Webb WR. Thin-section CT of the secondary pulmonary lobule: anatomy and the image—the 2004 Fleischner Lecture. *Radiology* 2006;239:322–338.
- Hogg JC, Chu F, Utokaparch S, Woods R, Elliott WM, Buzatu L, et al. The nature of small-airway obstruction in chronic obstructive pulmonary disease. *N Engl J Med* 2004;350:2645–2653.
- McDonough JE, Yuan R, Suzuki M, Seyednejad N, Elliott WM, Sanchez PG, et al. Small-airway obstruction and emphysema in chronic obstructive pulmonary disease. *N Engl J Med* 2011;365:1567–1575.
- Tanabe N, Vasilescu DM, McDonough JE, Kinose D, Suzuki M, Cooper JD, et al. Micro-computed tomography comparison of preterminal bronchioles in centrilobular and panlobular emphysema. *Am J Respir Crit Care Med* 2017;195:630–638.
- Koo HK, Vasilescu DM, Booth S, Hsieh A, Katsamenis OL, Fishbane N, et al. Small airways disease in mild and moderate chronic obstructive pulmonary disease: a cross-sectional study. *Lancet Respir Med* 2018;6:591–602.
- Tanabe N, Vasilescu DM, Kirby M, Coxson HO, Verleden SE, Vanaudenaerde BM, et al. Analysis of airway pathology in COPD using a combination of computed tomography, micro-computed tomography and histology. *Eur Respir J* 2018;51:1701245.
- Galbán CJ, Han MK, Boes JL, Chughtai KA, Meyer CR, Johnson TD, et al. CT-based biomarker provides unique signature for diagnosis of COPD phenotypes and disease progression. *Nat Med* 2012;18:1711–1715.
- Bhatt SP, Soler X, Wang X, Murray S, Anzueto AR, Beaty TH, et al.; COPDGene Investigators. Association between functional small airway disease and FEV₁ decline in chronic obstructive pulmonary disease. *Am J Respir Crit Care Med* 2016;194:178–184.
- Vasilescu DM, Martinez FJ, Marchetti N, Galbán CJ, Hatt C, Meldrum CA, et al. Noninvasive imaging biomarker identifies small airway damage in severe chronic obstructive pulmonary disease. *Am J Respir Crit Care Med* 2019;200:575–581.
- Vogelmeier CF, Criner GJ, Martinez FJ, Anzueto A, Barnes PJ, Bourbeau J, et al. Global strategy for the diagnosis, management, and prevention of chronic obstructive lung disease 2017 report. GOLD executive summary. *Am J Respir Crit Care Med* 2017;195:557–582.
- Rustam S, Hu Y, Mahjour SB, Randell SH, Rendeiro AF, Ravichandran H, et al. A unique cellular organization of human distal airways and its disarray in chronic obstructive pulmonary disease [preprint]. bioRxiv; 2022 [accessed 2023 Feb 16]. Available from: <https://doi.org/10.1101/2022.03.16.484543>.
- Hao Y, Hao S, Andersen-Nissen E, Mauck WM III, Zheng S, Butler A, et al. Integrated analysis of multimodal single-cell data. *Cell* 2021;184:3573–3587.e29.
- McGinnis CS, Murrow LM, Gartner ZJ. DoubletFinder: doublet detection in single-cell RNA sequencing data using artificial nearest neighbors. *Cell Syst* 2019;8:329–337.e4.
- Yang J, Zuo W-L, Fukui T, Chao I, Gomi K, Lee B, et al. Smoking-dependent distal-to-proximal repatterning of the adult human small airway epithelium. *Am J Respir Crit Care Med* 2017;196:340–352.
- Zuo WL, Yang J, Gomi K, Chao I, Crystal RG, Shaykhiiev R. EGF-amphiregulin interplay in airway stem/progenitor cells links the pathogenesis of smoking-induced lesions in the human airway epithelium. *Stem Cells* 2017;35:824–837.
- Shaykhiiev R, Zuo W-L, Chao I, Fukui T, Witover B, Brekman A, et al. EGF shifts human airway basal cell fate toward a smoking-associated airway epithelial phenotype. *Proc Natl Acad Sci USA* 2013;110:12102–12107.
- Carraro G, Langerman J, Sabri S, Lorenzana Z, Purkayastha A, Zhang G, et al. Transcriptional analysis of cystic fibrosis airways at single-cell resolution reveals altered epithelial cell states and composition. *Nat Med* 2021;27:806–814.
- García SR, Deprez M, Lebrigand K, Cavard A, Paquet A, Arguel MJ, et al. Novel dynamics of human mucociliary differentiation revealed by single-cell RNA sequencing of nasal epithelial cultures. *Development* 2019;146:dev177428.

21. Deprez M, Zaragosi LE, Truchi M, Becavin C, Ruiz García S, Arguel MJ, *et al*. A single-cell atlas of the human healthy airways. *Am J Respir Crit Care Med* 2020;202:1636–1645.
22. Vieira Braga FA, Kar G, Berg M, Carpaij OA, Polanski K, Simon LM, *et al*. A cellular census of human lungs identifies novel cell states in health and in asthma. *Nat Med* 2019;25:1153–1163.
23. Montoro DT, Haber AL, Biton M, Vinarsky V, Lin B, Birket SE, *et al*. A revised airway epithelial hierarchy includes CFTR-expressing ionocytes. *Nature* 2018;560:319–324.
24. Plasschaert LW, Zilionis R, Choo-Wing R, Savova V, Knehr J, Roma G, *et al*. A single-cell atlas of the airway epithelium reveals the CFTR-rich pulmonary ionocyte. *Nature* 2018;560:377–381.
25. Travaglini KJ, Nabhan AN, Penland L, Sinha R, Gillich A, Sit RV, *et al*. A molecular cell atlas of the human lung from single-cell RNA sequencing. *Nature* 2020;587:619–625.
26. Kumar BV, Connors TJ, Farber DL. Human T cell development, localization, and function throughout life. *Immunity* 2018;48:202–213.
27. Szabo PA, Levitin HM, Miron M, Snyder ME, Senda T, Yuan J, *et al*. Single-cell transcriptomics of human T cells reveals tissue and activation signatures in health and disease. *Nat Commun* 2019;10:4706.
28. Kumar BV, Ma W, Miron M, Granot T, Guyer RS, Carpenter DJ, *et al*. Human tissue-resident memory T cells are defined by core transcriptional and functional signatures in lymphoid and mucosal sites. *Cell Rep* 2017;20:2921–2934.
29. Angelidis I, Simon LM, Fernandez IE, Strunz M, Mayr CH, Greiffo FR, *et al*. An atlas of the aging lung mapped by single cell transcriptomics and deep tissue proteomics. *Nat Commun* 2019;10:963.
30. Strunz M, Simon LM, Ansari M, Kathiriya JJ, Angelidis I, Mayr CH, *et al*. Alveolar regeneration through a Krt8⁺ transitional stem cell state that persists in human lung fibrosis. *Nat Commun* 2020;11:3559.
31. Plopper CG, Hill LH, Mariassy AT. Ultrastructure of the nonciliated bronchiolar epithelial (Clara) cell of mammalian lung. III. A study of man with comparison of 15 mammalian species. *Exp Lung Res* 1980;1:171–180.
32. ten Have-Opbroek AA, Otto-Verberne CJM, Dubbeldam JA, Dijkman JH. The proximal border of the human respiratory unit, as shown by scanning and transmission electron microscopy and light microscopical cytochemistry. *Anat Rec* 1991;229:339–354.
33. Reynolds SD, Reynolds PR, Pryhuber GS, Finder JD, Stripp BR. Secretoglobins SCGB3A1 and SCGB3A2 define secretory cell subsets in mouse and human airways. *Am J Respir Crit Care Med* 2002;166:1498–1509.
34. Rock JR, Randell SH, Hogan BLM. Airway basal stem cells: a perspective on their roles in epithelial homeostasis and remodeling. *Dis Model Mech* 2010;3:545–556.
35. Hajj R, Baranek T, Le Naour R, Lesimple P, Puchelle E, Coraux C. Basal cells of the human adult airway surface epithelium retain transit-amplifying cell properties. *Stem Cells* 2007;25:139–148.
36. Bal HS, Ghoshal NG. Morphology of the terminal bronchiolar region of common laboratory mammals. *Lab Anim* 1988;22:76–82.
37. Basil MC, Cardenas-Diaz FL, Kathiriya JJ, Morley MP, Carl J, Brumwell AN, *et al*. Human distal airways contain a multipotent secretory cell that can regenerate alveoli. *Nature* 2022;604:120–126.
38. Kadur Lakshminarasimha Murthy P, Sontake V, Tata A, Kobayashi Y, Macadlo L, Okuda K, *et al*. Human distal lung maps and lineage hierarchies reveal a bipotent progenitor. *Nature* 2022;604:111–119.
39. Kumar PA, Hu Y, Yamamoto Y, Hoe NB, Wei TS, Mu D, *et al*. Distal airway stem cells yield alveoli in vitro and during lung regeneration following H1N1 influenza infection. *Cell* 2011;147:525–538.
40. Okuda K, Chen G, Subramani DB, Wolf M, Gilmore RC, Kato T, *et al*. Localization of secretory mucins MUC5AC and MUC5B in normal/healthy human airways. *Am J Respir Crit Care Med* 2019;199:715–727.
41. Adams TS, Schupp JC, Poli S, Ayaub EA, Neumark N, Ahangari F, *et al*. Single-cell RNA-seq reveals ectopic and aberrant lung-resident cell populations in idiopathic pulmonary fibrosis. *Sci Adv* 2020;6:eaba1983.
42. Schupp JC, Adams TS, Cosme C Jr, Raredon MSB, Yuan Y, Omote N, *et al*. Integrated single-cell atlas of endothelial cells of the human lung. *Circulation* 2021;144:286–302.
43. Jessen KR, Mirsky R, Lloyd AC. Schwann cells: development and role in nerve repair. *Cold Spring Harb Perspect Biol* 2015;7:a020487.
44. Gillich A, Zhang F, Farmer CG, Travaglini KJ, Tan SY, Gu M, *et al*. Capillary cell-type specialization in the alveolus. *Nature* 2020;586:785–789.
45. Saetta M, Di Stefano A, Turato G, Facchini FM, Corbino L, Mapp CE, *et al*. CD8⁺ T-lymphocytes in peripheral airways of smokers with chronic obstructive pulmonary disease. *Am J Respir Crit Care Med* 1998;157:822–826.
46. Xu F, Vasilescu DM, Kinose D, Tanabe N, Ng KW, Coxson HO, *et al*. The molecular and cellular mechanisms associated with the destruction of terminal bronchioles in COPD. *Eur Respir J* 2022;59:2101411.
47. Shaykhiev R. Airway epithelial progenitors and the natural history of chronic obstructive pulmonary disease. *Am J Respir Crit Care Med* 2018;197:847–849.
48. Staudt MR, Buro-Auriemma LJ, Walters MS, Salit J, Vincent T, Shaykhiev R, *et al*. Airway basal stem/progenitor cells have diminished capacity to regenerate airway epithelium in chronic obstructive pulmonary disease. *Am J Respir Crit Care Med* 2014;190:955–958.
49. Rao W, Wang S, Duleba M, Niroula S, Goller K, Xie J, *et al*. Regenerative metaplastic clones in COPD lung drive inflammation and fibrosis. *Cell* 2020;181:848–864.e18.
50. Ballarin A, Bazzan E, Zenteno RH, Turato G, Baraldo S, Zanovello D, *et al*. Mast cell infiltration discriminates between histopathological phenotypes of chronic obstructive pulmonary disease. *Am J Respir Crit Care Med* 2012;186:233–239.